

# MULTI-SCALE MODELLING OF DETERIORATING CONCRETE AT ELEVATED TEMPERATURE AND COLLAPSE SIMULATION OF UNDERGROUND DUCTS

KEITAI IWAMA<sup>\*</sup>, KAZUAKI HIGUCHI<sup>\*</sup> AND KOICHI MAEKAWA<sup>†</sup>

<sup>\*</sup> Graduate School of Urban Innovation, Yokohama National University  
79-5, Tokiwadai, Hodogaya, Yokohama, Japan  
e-mail: iwama-keitai-cm@ynu.jp  
higuchi-kazuaki-wj@ynu.jp

<sup>†</sup> Department of Civil Engineering, Yokohama National University  
79-5, Tokiwadai, Hodogaya, Yokohama, Japan  
e-mail: maekawa-koichi-tn@ynu.ac.jp

**Key words:** Multi-scale modelling, Fire, Dehydration, Failure mode, Underground duct

**Abstract:** Based on the multi-scale platform of cementitious composite, the release of chemically bound water of  $\text{Al}_2\text{O}_3\text{-Fe}_2\text{O}_3\text{-mono}$  (AFm), calcium silicate hydrate (CSH) and calcium hydroxide (CH) is developed by micro-pore structural modelling and rehydration of CH crystals is linked under cyclic fire and wetting. This framework is further improved to handle the spalling of concrete cover against fire hazards. The strength of CSH solid at micro-level and that of concrete composite of meso-level are numerically presented. The collapse simulation of underground ducts exposed to fire is conducted by the developed multi-scale analysis which is also integrated with soil foundation. It predicts varying mode of failure associated with spalling of cover concrete and the loss of bond.

## 1 INTRODUCTION

The fire damage is the thermo-chemo-mechanical event of structural concrete. Decomposition of cement hydrate solids, strength decay of concrete and reinforcing bars, developing explosive cracks and consequent spalling of concrete may occur when concrete structures are exposed to fire.

There are innumerable experiences of thermo-chemo-mechanics of concrete exposed to high temperature and fire [1-4]. Previous researches [5-8] try to predict the spalling of concrete which is one of significant factors of structural deterioration at fire by considering the thermal stress and the rising vapour pressure. In the past investigations, the variety of concrete composite could be hardly taken into account since heat hydration and the solidification processes at micro-scale were not linked with macro-behavioural simulation of

structural concrete. Thus, the post-spalling safety assessment has been mostly performed experimentally.

To satisfy the multifaceted requirements, performance assessment is essential on the scheme of limit state design. Thus, the multi-scale model to computationally reproduce structural responses after spalling is expected to practically function for the risk assessment of fire hazards.

Based on the multi-scale platform [9-10] of cementitious composites, the deterioration of both calcium silicate hydrate (CSH) and calcium hydroxide (CH) solids accompanying varying micro-pores is formulated under high temperature at fire, and the macroscopic simulation of structural concrete [10] is presented for safety assessment of underground urban spaces. The micro-pore structural modelling is developed in consideration of the

release of chemically bound water, and rehydration of CH crystals is integrated under cyclic fire and wetting [11]. This modelling of microscopic porous solid is combined with meso-scale thermodynamics of moisture. The deformation and fracture of solid skeletons are integrated with the macroscopic constitutive models for cracked concrete [10]. This framework is originated to handle the spalling of concrete cover and the exposure of reinforcing bars to fire. Here, the mechanical properties of hardened concrete are computed based upon the micro-pore structures which may mature at curing and decompose at fire.

In this paper, the authors apply this multi-scale modelling for structural risk assessment of underground utility ducts surrounded by soil foundation at fire. To investigate the structural behaviours after spalling, this framework is upgraded in order to handle the continuous spalling of concrete cover against fire and validated by meso-scale experimental results. Thereafter, collapse simulation of underground ducts from fire is performed so that we may indicate the conversion of its failure mode from shear to flexure.

## 2 DECOMPOSITION AT HIGH TEMPERATURE AND REHYDRATION

### 2.1 Dehydrated AFm, CSH and CH and rehydrated CH

The dehydration of AFm and CSH takes place comparatively in lower temperature at fire. The crystallized water of AFm is decomposed at the beginning of temperature rise. Further, the crystallized water of CSH is dehydrated when temperature rises more than 200°C. In the present model, it is simply assumed that the decomposition of AFm starts from 100°C and the decomposition of CSH begins at about 200°C. By considering the application to the structural analysis at fire, we have:

$$W_{d(AFm)} = W_{c(AFm)} \left( 1 - \sqrt{\frac{100}{T_{\max}(AFm)}} \right) \quad (1)$$

$$W_{d(CSH)} = W_{c(CSH)} \left( 1 - \sqrt{\frac{200}{T_{\max}(CSH)}} \right) \quad (2)$$

where,  $W_{d(AFm)}$  is the weight loss of crystallized water of AFm (% by unit weight of cement),  $W_{c(AFm)}$  is crystallized water of AFm (% by unit

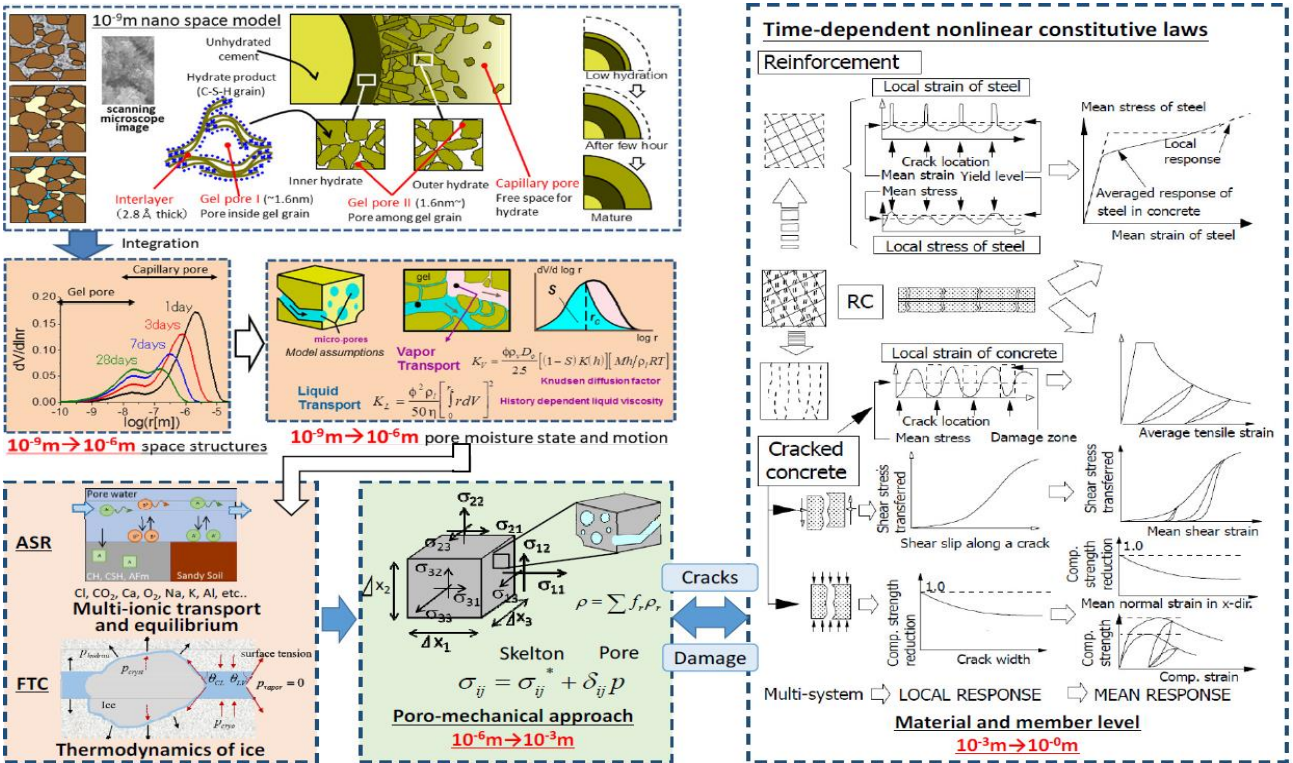


Figure 1: Outline of multi-scale modelling of structural concrete.

weight of cement),  $T_{max(AFm)}$  is the maximum temperature for AFm which experienced in the past ambient history ( $\geq 100^\circ\text{C}$ ),  $W_{d(CSH)}$  is the weight loss of crystallized water of CSH (% by unit weight of cement),  $W_{c(CSH)}$  is the crystallized water of CSH (% by unit weight of cement),  $T_{max(CSH)}$  is the maximum temperature for CSH which experienced in the past ambient history ( $\geq 200^\circ\text{C}$ ).

The weight loss percentage of crystallized water is calculated by Equations (2) and (3), and its absolute weight loss ( $\text{kg/m}^3$ ) is computed with these percentages and the amount of crystallized water computed by integrating the rate of the cement hydration linked with the microstructure development of the multi-scale hygro-chemo-physics (Figure 1). According to these results, the porosity of capillary pores increases as the cement hydrates are partially broken and the space occupied by the chemically bound water is released as shown in Figure 2.

The porosity owing to released crystallized water is logically the same as the one calculated from the microstructure development model [9], since the hydrates whose crystallized water were released are the pores in microstructure

development model. The consistency of mass was experimentally confirmed.

It is well known that the decomposition of pure CH solid takes place from around  $400^\circ\text{C}$  [12]. First, the characteristics of decomposed pure single CH is installed in the model framework and a sudden drop of chemically bound water when temperature rises from  $400^\circ\text{C}$  to  $450^\circ\text{C}$  is assumed as:

$$W_{d(CH)} = W_{c(CH)} \left( \frac{T_{max} - 400}{50} \right) \quad (3)$$

where,  $W_{d(CH)}$  is the weight loss of crystallized water of CH ( $\text{kg/m}^3$ ),  $W_{c(CH)}$  is the one of CH ( $\text{kg/m}^3$ ), and  $T_{max}$  is the past experienced maximum temperature ( $400^\circ\text{C} \leq T_{max}$ ). Over  $450^\circ\text{C}$ , no further loss is assumed as:

$$W_{d(CH)} = W_{c(CH)} \quad (4)$$

In the case of CH, the calculated porosity of capillary pores is idealized as the same as AFm and CSH.

Although the rehydration process [13] for post-fire curing is insignificant in practice, the authors include this chemical process as a fundamental thermodynamic event within the multi-scale scheme of pore evolution and

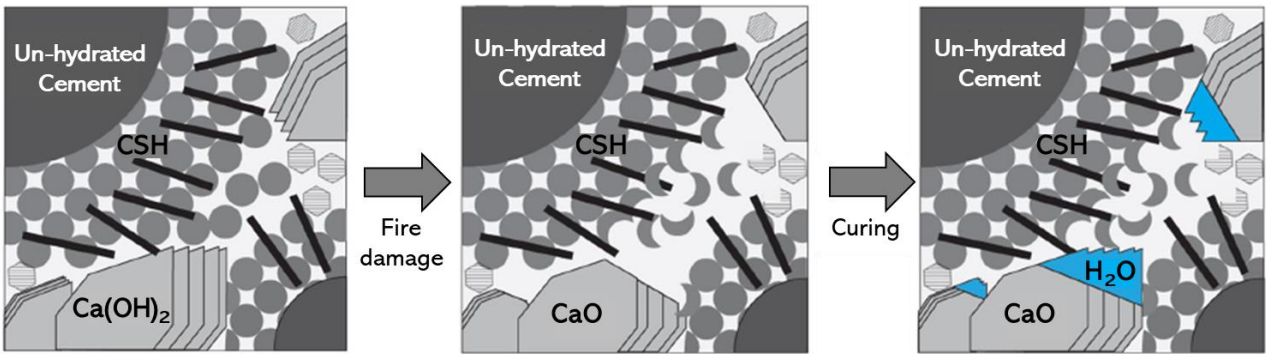


Figure 2: Explanation of dehydration and rehydration model.

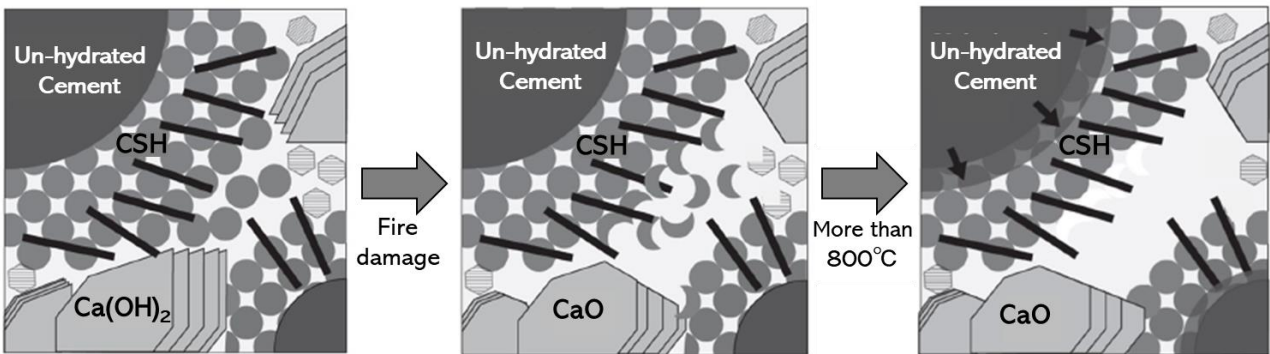


Figure 3: Explanation of re-clinker model of damaged CSH.

degradation as shown in Figure 2. It is assumed that the highly reactive CaO be just rehydrated, but the decomposed AFm and CSH may not revive even though the space occupied by them can be possibly filled up by new hydrates with free water when sufficient un-hydrated cement remains in the mixture.

## 2.2 Re-clinker model of damaged CSH

The re-clinker process which is defined as the revival process of dehydrated CSH to clinker is included in the proposed model. As shown in Figure 3, 1) revived CSH to clinker is already decomposed after release of the chemically bound water, 2) re-clinker may begin over 800°C, 3) all damaged CSH is assumed to revive to clinker kept in the temperature over 800°C for more than two hours, and 4) mass conservation and theoretical compatibility shall be satisfied since the amount of revived CSH to clinker never exceed the amount of decomposed CSH.

It must be noted that the re-clinker process is represented by so called inversed hydration, i.e.,

re-clinker is an increased un-hydrated cement. This process of the re-clinker event is described such that the hydration degree of the constituent mineral is “rebound” as:

$$\frac{dD_{CSH}}{dt} = -C \cdot D_{CSH} \quad (5)$$

$$D_{CSH} = D_{CSH(t=0)} \cdot \exp(-C \cdot t) \quad (6)$$

$$\alpha_{damage(t)} = [1 - (D_{CSH,0} - D_{CSH})] \cdot \alpha_0 \quad (7)$$

where,  $D_{CSH}$  is the ratio of the damaged CSH to those already created by heat hydration at the updated time ( $0 \leq D_{CSH} \leq 1$ ),  $t$  is the time of keeping the hydrates over 800°C (day),  $C$  specifies the rate factor of the reaction and its inverse means the representative half time ( $\text{day}^{-1}$ ),  $D_{CSH,0}$  is the ratio of damaged CSH to those already created by heat hydration at time zero ( $0 \leq D_{CSH(t=0)} \leq 1$ ),  $\alpha_{damage(t)}$  is the reversed degree of hydration associated with the re-clinker process at the time  $t$  ( $0 \leq \alpha_{damage(t)} \leq 1$ ) and  $\alpha_0$  is the hydration degree calculated at the time when the reaction is activated ( $0 \leq \alpha_0 \leq 1$ ).

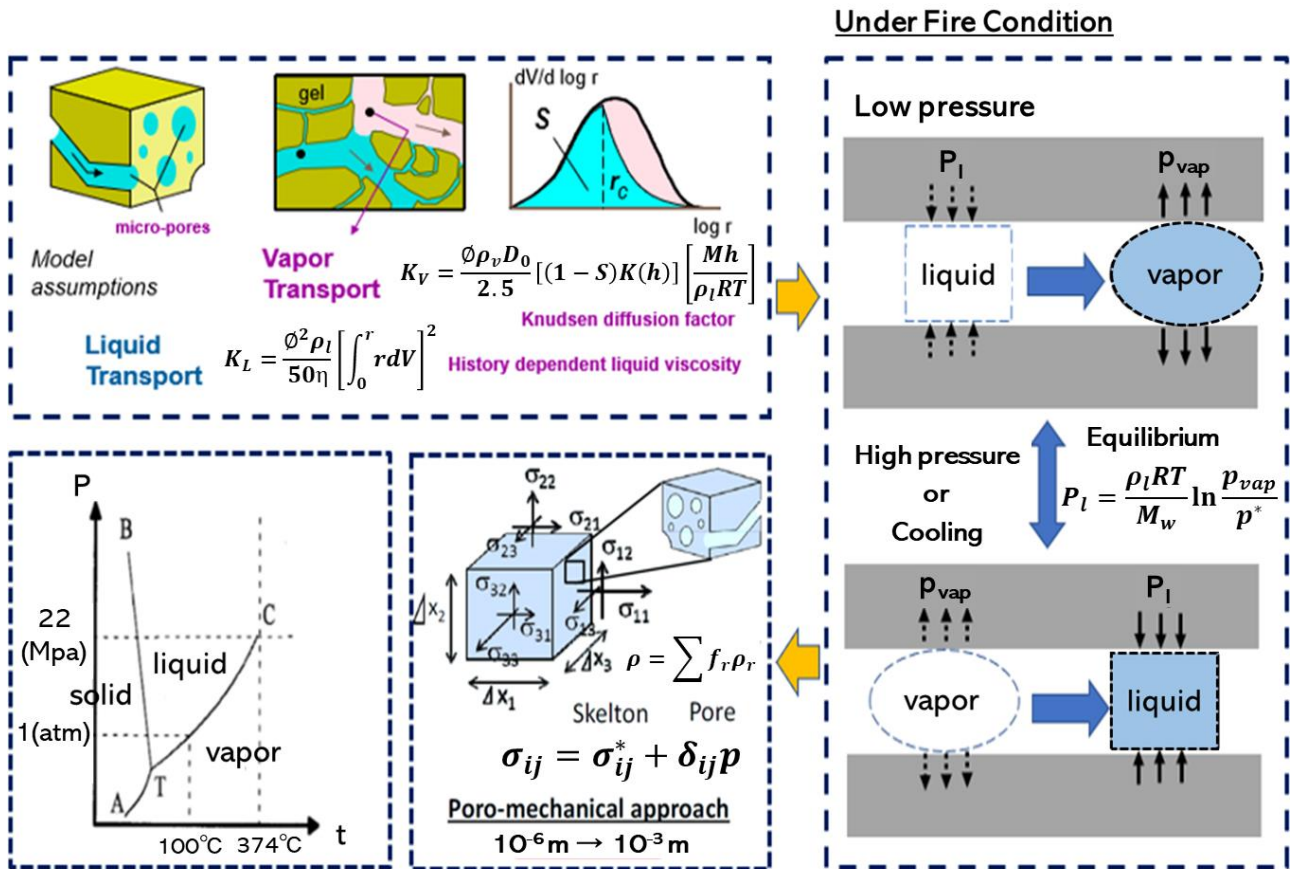


Figure 4: Consideration of pressure conditions under fire.

### 3 MODELLING OF SPALLING

#### 3.1 Vapour pressure inside micro-pores and criterion of spalling

The principal factors for fire damage of concrete are the thermal stress generated due to restraint of thermal expansion (self-equilibrated and externally confined), and the vapour pressure caused by vaporization of liquid water inside micro pores. The proposed model considers these factors and we have the total stresses of concrete solids and pore media as follows:

$$\sigma_{ij} = \sigma_{ij}' + \delta_{ij}p_{vap} \quad (8)$$

where,  $\sigma_{ij}$  is total stress (Pa),  $\sigma_{ij}'$  is the effective stress tensor defined on the concrete skeleton (Pa) and  $p_{vap}$  is absolute vapour pressure inside pores and crack gaps (Pa). In the scheme of hygro-chemo-physics model, we the thermodynamic phase equilibrium of the idealized gas as,

$$p_{vap} = P_{sat} \exp\left(\frac{P_l M_w}{\rho_l R T}\right) \quad (9)$$

where,  $P_{sat}$  is saturated vapour pressure (Pa),  $P_l$  is pore-water pressure (Pa),  $M_w$  is molar volume of liquid water (kg/mol),  $\rho_l$  is density of liquid water (kg/m<sup>3</sup>),  $R$  is gas constant (J/mol/K) and  $T$  is absolute temperature (K).

As shown in Figure 4, moisture transfer is driven by both pressure and temperature gradients. Further, thermodynamic equilibrium between liquid and vapour is considered in the hygro-chemo-physics model [9] which incorporates both vaporization of heated liquid water and concentration of cooled or high-pressure vapour.

The total stress is calculated by solving the equilibrium equations of both solid skeleton and pore media, and the deformational compatibility where the increase of vapour pressure inside pore spaces, the thermal expansion of concrete and boundary conditions of external forces and displacement constraint. If computed tensile stress exceeds tensile strength of concrete, cracks take place normal to the principal stress direction. The larger the crack width develops, the easier the moisture transfer along the crack surface is [9,14].

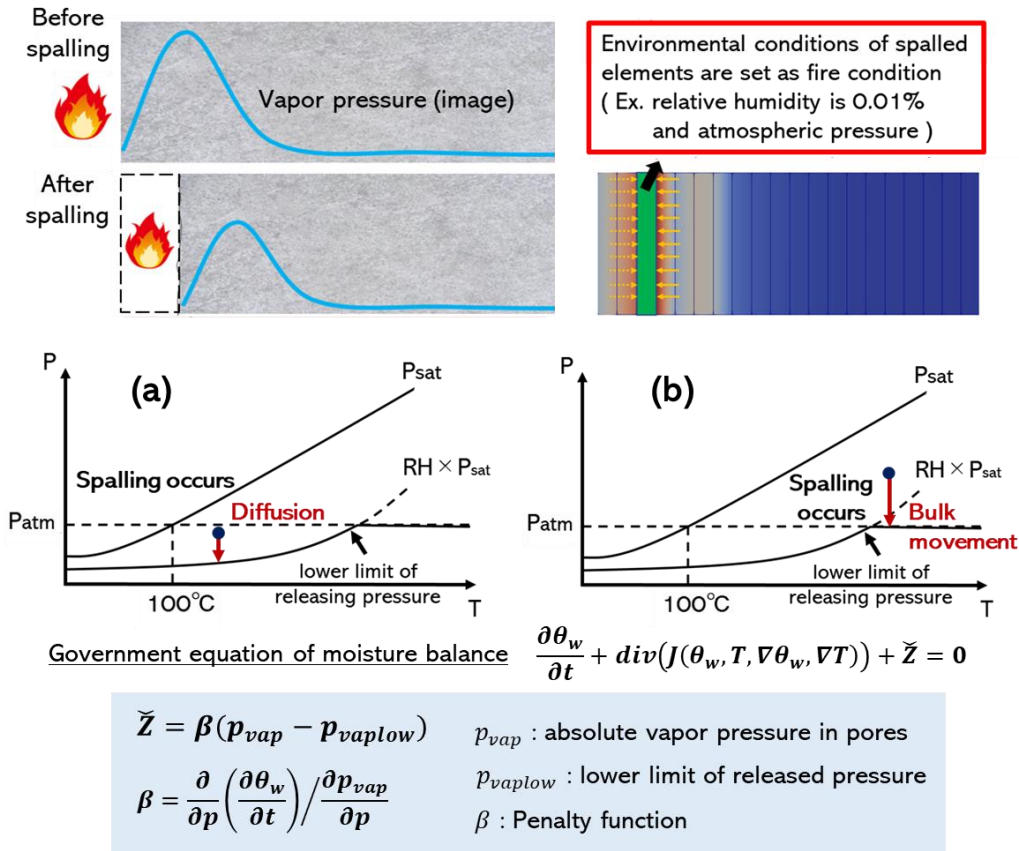


Figure 5: Modelling of concrete spalling under fire.

The intrinsic vapour pressure (V-PRS) corresponding to no volume change and the effective vapour one associated with the volume change (E-PRS) of the finite element domain are calculated in the hygro-chemo-physics model [9] and the structural concrete including cracks.

E-PRS decreases when crack or the large volume expansion occurs. In this paper, we simply apply the ideal gas law by assuming that the vapour pressure inside capillary pores and that of the spaces of crack gaps are equal. The occurrence of spalling can be simply identified based on the difference of V-PRS and E-PRS. When the pressure drop (the difference of V-PRS and E-PRS) is less at the time of crack occurrence, we can judge that the cracked concrete still remains as a part of the whole structure. When the pressure release is large enough to exceed some limit state, the cracked concrete may depart from the structural concrete so that the vapour pressure and temperature of the volume occupied by the lost concrete come up the external ambient states.

### 3.2 Continuous spalling one after another

As shown in Figure 5, piece of concreted parts from the structural surface when spalling occurs. As FEM assumes continuum fields, it is hard to reproduce geometrically vanishing elements. Instead, we may have thermo-mechanically equivalent states for post-spalling of concrete. The vapour pressure of domains

occupied by spalling element is forced to be equal to the ambient one. It means that the remaining core concrete is exposed to the external environments after spalling. This numerical process may thermodynamically kill the mechanism of mass transport and conservation of lost concrete after spalling. Since the strain is large, the stress transfer mechanism is automatically lost. Then, the impact of spalling of concrete can be reproduced in simulation.

This process is performed by adding  $\tilde{Z}$  to the transient rate-type governing equation of moisture conservation [9] as:

$$\frac{\partial \theta_w}{\partial t} + \text{div}(J(\theta_w, T, \nabla \theta_w, \nabla T)) + \tilde{Z} = 0 \quad (10)$$

$$\tilde{Z} = \beta(p_{vap} - p_{vaplow}) \quad (11)$$

$$\beta = \frac{\frac{\partial}{\partial p} \left( \frac{\partial \theta_w}{\partial t} \right)}{\frac{\partial p_{vap}}{\partial p}} = \frac{\partial^2 \theta_w}{\partial p \partial t} / \frac{\partial p_{vap}}{\partial p} \quad (12)$$

where,  $\tilde{Z}$  is the rate of moisture mass which is released to outside of concrete per unit time ( $\text{kg}/(\text{m}^3 \cdot \text{s})$ ),  $p_{vap}$  is the absolute vapour pressure (Pa),  $p_{vaplow}$  is the lower limit of released pressure (Pa),  $P_{atm}$  is the atmospheric pressure ( $=1.0 \times 10^5 \text{Pa}$ ) and  $\beta$  is the penalty function so as to stabilize the pore pressure converging to the external environment.

When spalling occurs, the velocity of moisture transport is determined by the difference between the absolute vapour pressure and the lower limit of released one

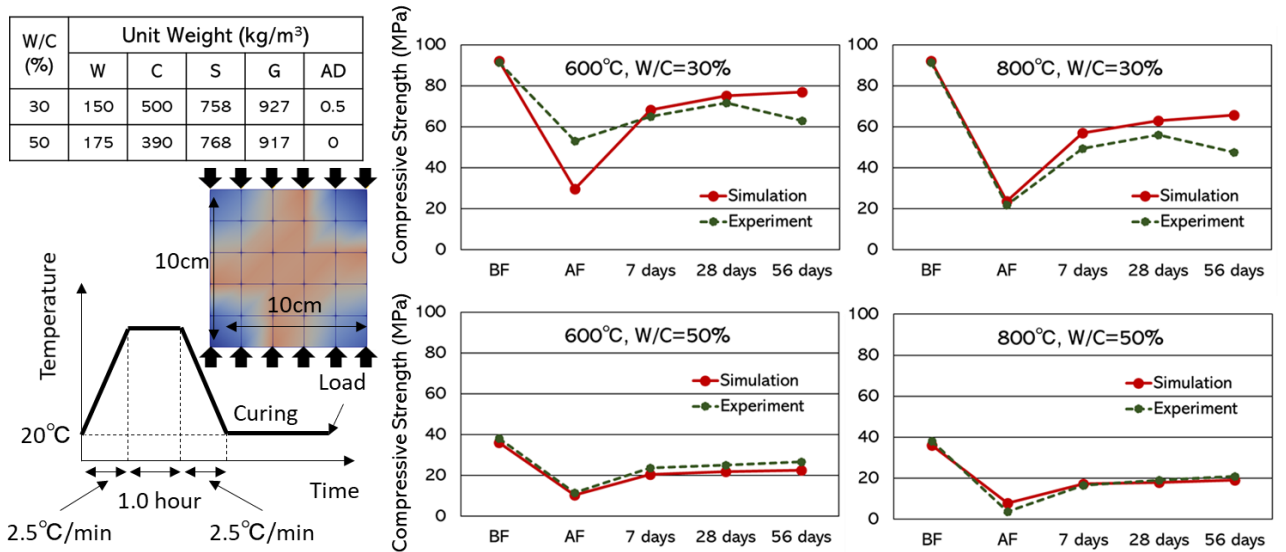


Figure 6: Comparison of compressive strength with experiment about post-fire-curing by cube model.

whose maximum is the atmospheric pressure. In the condition illustrated in Figure 5 (a),  $p_{vaplow}$  is set up to be  $P_{atm}$  and the moisture is transported by bulk movement. On the other hand, in the condition shown in Figure 5 (b),  $p_{vaplow}$  is not equal to  $P_{atm}$  and moisture is transported by diffusion.

As shown in equation (12), penalty function  $\beta$  is expressed by the ratio of the pressure differential of change in total water content ( $\partial^2\theta_w/\partial t/\partial p$ ) to the pressure differential of absolute vapour pressure ( $\partial p_{vap}/\partial p$ ). Both the change in total water content and moisture mass released into outside of concrete per unit time are the function of pore pressure. Their summation defines the moisture content of concrete. Considering the sensitivity of  $\partial^2\theta_w/\partial t/\partial p$  and  $\partial p_{vap}/\partial p$ , the vapour pressure easily approaches to the lower limit of the released pressure with high stability.

## 4 VALIDATION OF THE PROPOSED MODEL THROUGH EXPERIMENTAL INVESTIGATIONS

### 4.1 Validation of compressive strength by concrete cubes

The established model explained in Section 2 and Section 3 is validated by using previous experimental results [13].

In the experiment, compressive strength test was performed on 100mm concrete cubes. There were two mix proportions considering 30% and 50% water to cement ratio (W/C) as shown in Figure 6. The specimens were demolded after 24 hours of casting and emerged into water ensured at 20°C. After 28 days of water curing, the specimens were transferred into an environmental chamber maintaining 20°C and 75% relative humidity (RH). At the age of 60 days, the specimens were heated in an electric furnace up to 600°C and 800°C which are kept constant for one hour. The heating and cooling rate was set as 2.5°C/min. The specimens were cooled down naturally to 20°C after the completion of heating cycle. Then the specimens were kept in 20°C for 12 hours.

As shown in Figure 6, compressive strength tests were performed before fire (BF), after fire (AF) and at 7<sup>th</sup> day, 28<sup>th</sup> day and 56<sup>th</sup> day of

post-fire-curing time of the specimens respectively. Figure 6 shows the comparison of experimental and simulation results. Compressive strength decreases after heating and recovers after post-fire-curing. These results confirm the accuracy of the proposed model in predicting the decline and the recovery behaviour of the compressive strength of concrete. However, the simulation results of AF for 600°C-W/C=30% differs from the experimental result, while the simulation results of AF for 800°C-W/C=30% corresponds with the experimental result. It means that the fire damage by vapour pressure is larger in case of simulation than that of experimental result because vapour pressure in simulation is difficult to reduce as compared to the test specimens.

Further, the experimental compressive strength at 56<sup>th</sup> day for W/C=30% is exceptionally decreased compared to that of 28<sup>th</sup> day. In case of low water to cement ratio, hydration of un-hydrated cement and rehydration of dehydrated cement hydrates will occur at the same time. Therefore, it is considered that the generation amount of hydrates becomes large beyond recovery and breaks the internal micro structure.

### 4.2 Microscopic strength of CSH solids and meso-scale concrete composite

The degree of hydration of each mineral is calculated by multi-component hydration heat model. Based on the degree of hydration, cement hydrates are created by the microstructure development model [9]. As shown in upper part of Figure 7, the microstructure gradually gets dense followed by the decreased capillary pores. Presently, the strength is simply assessed by the capillary pore porosity [15]. In this paper, the computed strength based on the reduction of porosity of capillary pore is defined as the microscopic strength of CSH solids.

The compressive strength of concrete is obtained by the compressive strength test in general. This strength incorporates structural factors such as development of cracks, fracture of micro structures, etc. In the multi-scale

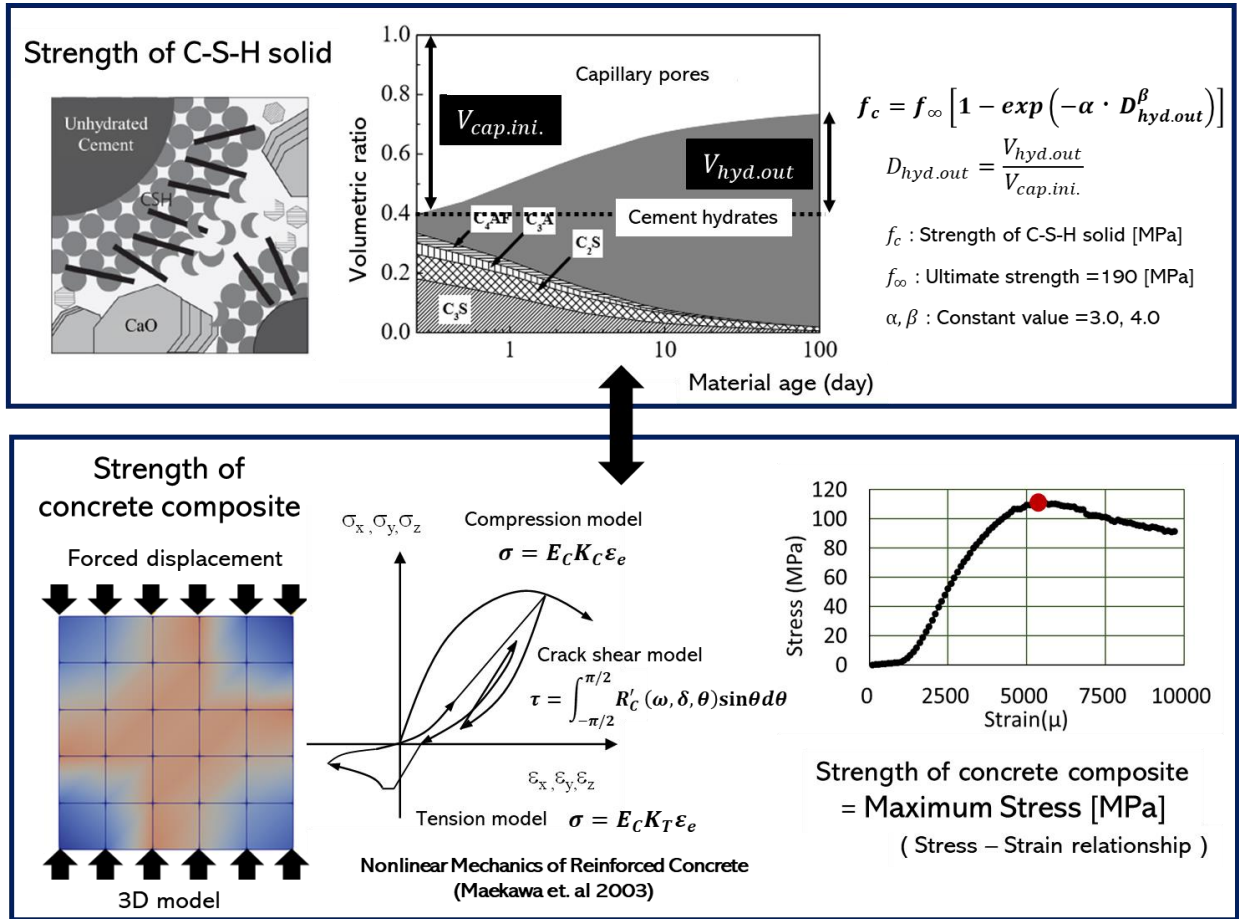


Figure 7: Definition of strength of CSH solid and strength of concrete composite.

modelling, nonlinear structural analysis linked with hygro-chemo-physics model can be conducted. As shown in lower part of Figure 7, compressive strength test can be simulated by 3D finite element model and compressive strength can be obtained from calculated stress-strain behaviour. In the present paper, the obtained strength is defined as the strength of concrete composite.

The microscopic strength of CSH solids and concrete composite are different. The strength of concrete composite is decreased by the structural damages like micro cracks, thermal expansion etc. although the microscopic strength of CSH solids is remained same. Therefore, as shown in Figure 8, strength ratio is defined as the ratio of the strength of concrete composite to the microscopic strength of CSH solids. This strength ratio is considered as an index to investigate the structural damage of concrete at high temperature due to fire.

The simulation models are 100mm concrete cubes and mix proportions are W/C=30% and

50%. The heating and cooling rate is set as 2.5°C/min and then the specimens were kept at 20°C for 12 hours. Then, compressive strength test is conducted and strength of concrete composite is obtained. Microscopic strength of CSH solids is calculated just before the compressive strength test.

Figure 8 shows comparison of the strength ratio between the models before (model-BS) and after (model-AS) introduction of concrete spalling model explained in 3.2. According to the results from model-BS (Ratio-W/C=30%-no-spalling-model and Ratio-W/C=50%-no-spalling-model), strength ratio gradually decreases as the temperature rises. On the other hand, from model-AS (Ratio-W/C=30% and Ratio-W/C=50%), the decline of strength ratio stops from around 500°C. The internal damage is accumulated and the strength of concrete composite is decreased since the vapour pressure is not released in model-BS. Conversely, in model-AF, the internal damage is reduced due to the release of vapour pressure.

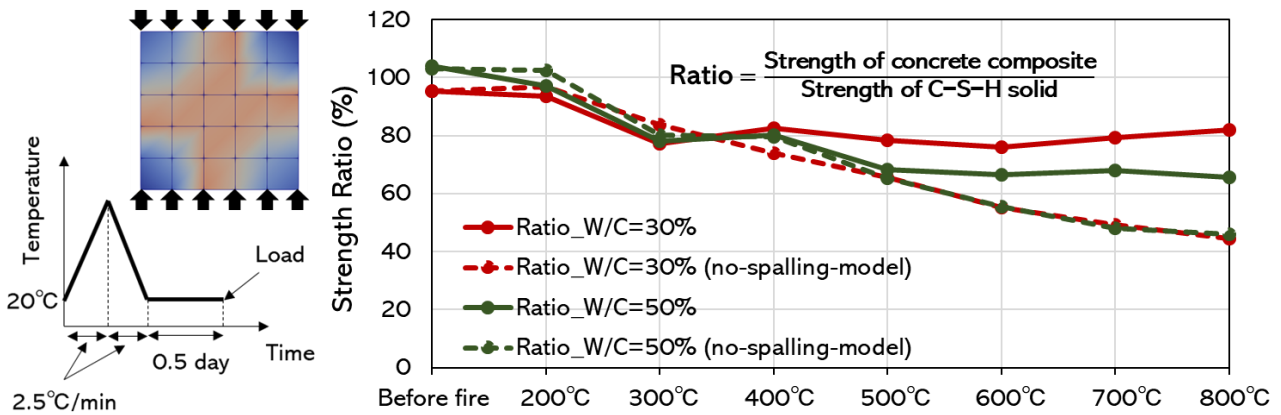


**Figure 8:** Comparison with strength of CSH solid and strength of concrete composite.

Moreover, according to the results of model-AS, the decline of strength ratio stops from around 300°C or 500°C. It indicates that strength decline of concrete is mainly affected by the structural factors caused by the applied temperature. However, the strength is mainly decreased due to the decline of microscopic strength of CSH solids at temperature larger than 500°C.

## 5 SAFETY ASSESSMENT OF UNDERGROUND DUCTS

### 5.1 Simulation model

Underground structures play an important role in urban areas which are now highly susceptible to fires, since they have been kept in a long service life and soil pressure. In fact, these infrastructures are hard to be repaired nor replaced. These underground stocks are reported to be damaged by long-term earth pressure, land subsidence and water infiltration.

On the contrary, underground spaces are safely protected against great earthquakes owing to the mutual nonlinear interaction of structural concrete and soil foundation. Then, we set up the coupled system of analysis as shown in Figure 9 to practically reveal the behaviours of underground structures at the event of fire under the influence of surrounding soil. The previous analysis model of finite element discretization [16] is improved for this simulation.

It is a reinforced concrete structure with W/C=63%, and it has been damaged due to ground subsidence and deteriorated due to drying shrinkage for 50 years. In the simulation,

a fire environment is applied to the surface of the RC duct after its 50 years of service period with uniform heating conditions. The long-term land subsidence is computationally reproduced in the simulation by applying downward forced displacement to the ground as shown in Figure 9 [15]. The maximum temperature of time-history of fire is set forth as 1200°C with a heating rate of 240°C/min for 48 hours.

### 5.2 Soundness of underground space at fire

According to the condition before fire (BF; see Figure 10), diagonal shear cracking is seen at the top corner of the RC duct in the ceiling slab and the wall. It should be noted that the real structure targeted by this model was investigated at site and the occurrence of shear cracking was definitely confirmed [16].

As shown in Figure 10, the further extension of the localized shear strain is not observed at the beginning stage of heating. Moreover, generation of thermal expansive strain was observed in two hours because of the heat volumetric expansion while the shear failure zone of the member does evolve. Thereafter, heating was continued. The heat was transmitted to the entire structural concrete in 48 hours and large deformation occurs due to the reduction of structural strength.

Previously, the final shear failure was forecasted over the section of the ceiling slabs, but the computed final failure mode is flexure. The reasons for the relaxation of localized shear strain zone and the failure mode transition from shear to flexure may attribute to the deteriorated bond of reinforcement and cover concrete, and

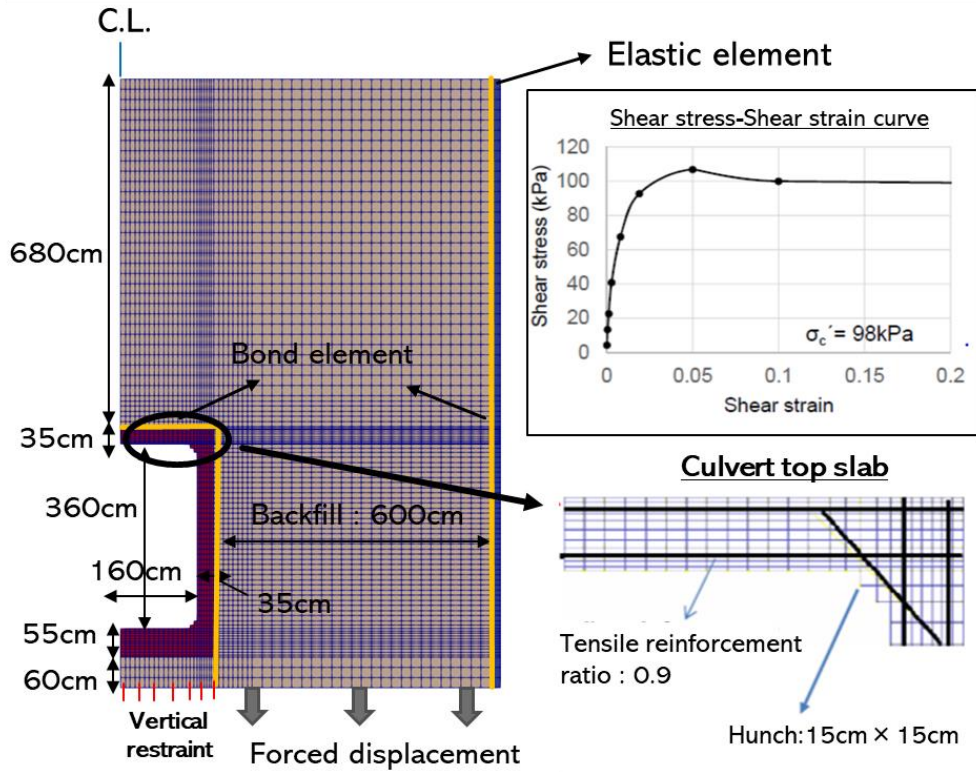


Figure 9: Two-dimensional model of the underground RC culvert.

the decrease in the yield strength of reinforcement at the high temperature environment. In fact, bond loss which is computationally made by spalling of cover is known to cause greater shear capacity of RC members. This mechanism has been pointed out experimentally and analytically in previous studies [17] as well.

Reduced yield strength of reinforcement at fire directly brings about the reduced flexural capacity as well. Then, the maximum possible shear force applied to the corner of the ducts is decreased as the shear capacity is equal to the gradient of bending moment. The gain of

member shear capacity at fire (related to spalling of concrete) and the reduced shear force (associated with the lower yield strength of reinforcement) are the mechanism of reduced risk of shear failure.

### 5.3 Failure mode of RC exposed to fire

As discussed in Section 5.2, there is a mechanical scenario of reduced risk of shear failure of structural members. At the same time, however, we have to consider the impact of the reduced compressive strength of concrete web at the elevated temperature. With this in view, the possible converted failure mode due to

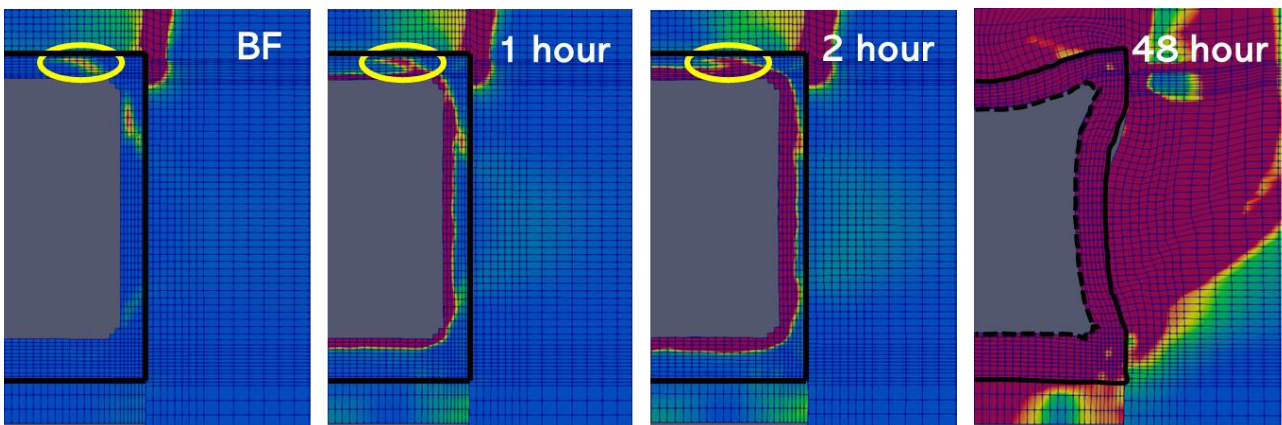
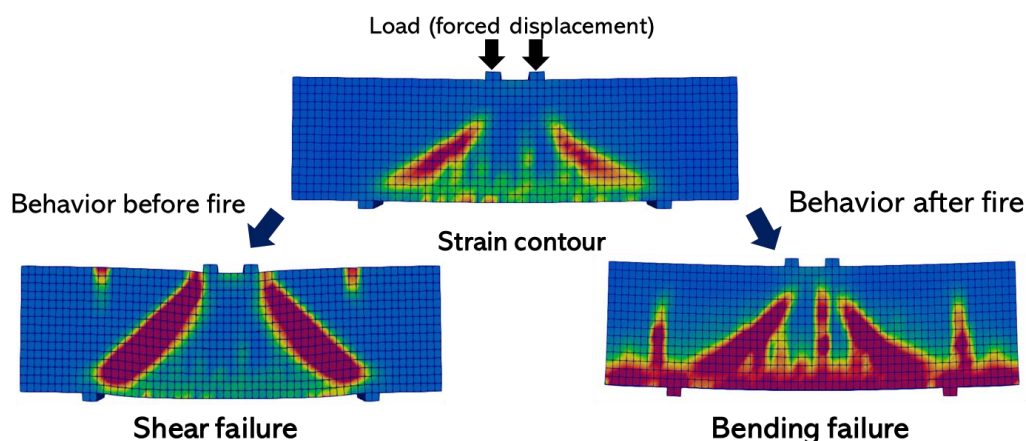


Figure 10: Fracture behaviour of the underground RC culvert at fire condition (displacement scale  $\times 1.0$ ).



**Figure 11:** Investigation of change of fracture mode by beam model (displacement scale  $\times 10$ ).

heating is investigated by focusing on simply supported RC beams as shown in Figure 11. The short shear span to depth ratio denoted by  $a/d$  is set forth as 1.4 so as to clearly reproduce the diagonal compression strut in shear. The mix proportion of concrete is the same as the underground duct whereas the longitudinal reinforcement ratio is defined as 1.67% to increase the flexural capacity. In the case of no-heating (left part of Figure 11), shear failure is confirmed accompanying the diagonal shear cracking as expected.

In the case of heating by fire (right part of Figure 11), first, the RC beam is loaded until the diagonal shear cracking appears and this load is suspended. Then, the bottom surface of the beam is heated as the underground duct was handled. As shown in Figure 11, the diagonal shear strain zone is not generated significantly.

On the other hand, flexural cracks develop significantly, and the failure mode has changed from shear to flexure as the underground duct failed. Anyhow, the reduced risk of shear failure is confirmed as well for the case of statically determinate member at fire. Within the authors' knowledge, the conversion of failure mode at fire is not experimentally substantiated. This point shall be discussed in future work.

## 6 CONCLUSIONS

The multi-scale modelling of chemo-physics and mechanics is extended to the higher temperature at fire and the following conclusions are earned as follows.

1) Dehydration model of cement hydrates and

concrete spalling model in high temperature at fire and rehydration model of dehydrated CH were incorporated in the multi-scale simulation platform. This modelling may reproduce both decay and recovery of meso-scale strength reasonably.

- 2) Microscopic strength of CSH solids is formulated based upon the deteriorated micro-pore structures associated with released crystallized water. The meso-scale strength of concrete composite is computed by combining the CSH strength and dispersed cracks in 3D extent.
- 3) The behavioural simulation of underground duct at fire was conducted, and the converted failure mode of structural members from shear to flexure was computationally predicted. This point shall be demonstrated in future experiments.

## REFERENCES

- [1] Ghan, Y.N., Peng, G.F. and Anson, M., 1999. Residual Strength and Pore Structure of High-strength Concrete and Normal Strength Concrete after Exposure to High Temperatures, *Cement and Concrete Composites*, Volume 21, Issue 1, 1999; pp.23-27.
- [2] Arioz, O., 2007. Effects of Elevated Temperatures on Properties of Concrete, *Fire Safety Journal*, Volume 42, Issue 8, November 2007; pp.516-522.
- [3] Phan, L.T., Lawson, J.R. and Davis, F.L., 2001. Effects of Elevated Temperature

- Exposure on Heating Characteristics, Spalling, and Residual Properties of High Performance Concrete, *Materials and Structures*, Volume 34, Issue 2, March 2001; pp.83-91.
- [4] Hertz, K.D., 2003. Limits of Spalling of Fire-exposed Concrete, *Fire Safety Journal*, Volume 38, Issue 2, March 2003; pp.103-116.
- [5] Majorana, C.E., Salomoni, V. and Schrefler, B.A., 1998. Hygrothermal and Mechanical Model of Concrete at High Temperature, *Materials and Structures*, Vol. 31, July 1998; pp.378-386.
- [6] Kalifa, P., Menneteau, F.D. and Quenard, D., 2000. Spalling and Pore Pressure in HPC at High Temperatures, *Cement and Concrete Research*, Volume 30, Issue 12, December 2000, pp.1915-1927.
- [7] Fu, Y., and Li, L., 2011. Study on Mechanism of Thermal Spalling in Concrete Exposed to Elevated Temperatures, *Materials and Structures*, Volume 44, Issue 1, January 2011; pp.361-376.
- [8] Gawin, D., Pesavento, F. and Schrefler, B.A., 2006. Towards Prediction of The Thermal Spalling Risk Through a Multi-Phase Porous Media Model of Concrete, *Computer Methods in Applied Mechanics and Engineering*, Volume 195, Issues 41-43, August 15, 2006; pp.5707-5729.
- [9] Maekawa, K., Ishida, T., and Kishi, T., 2008. *Multiscale Modeling of Structural Concrete*, Taylor & Francis.
- [10] Maekawa, K., Pimanmas, A., and Okamura, H., 2003. *Nonlinear Mechanics of Reinforced Concrete*, Spon Press.
- [11] Iwama, K., Ishibashi, N., and Maekawa, K., 2018. Modelling of Decomposition and Self-healing Processes of Hardened Cement Paste Exposed to High Temperature, *The 8th International Conference of Asian Concrete Federation*, Volume 1, November 4-7, 2018, Fuzhou, China; pp.227-234.
- [12] Vance, K., Falzone, G., Pignatelli, I., Bauchy, M., Balonis, M. and Sant, G., 2015. Direct Carbonation of Ca(OH)<sub>2</sub> Using Liquid and Supercritical CO<sub>2</sub>: Implications for Carbon-Neutral Cementation, *Industrial & Engineering Chemistry Research*, 54; pp.8908-8918.
- [13] Poon, C.S., Azhar, S., Anson, M. and Wong, Y.K., 2001. Strength and Durability Recovery of Fire-Damaged Concrete after Post-Fire-Curing, *Cement and Concrete Research*, 31; pp.1307-1318.
- [14] Bazant, Z.P., Sener, S. and Kim, J.K., 1987. Effect of Cracking on Drying Permeability and Diffusivity of Concrete, *ACI materials journal*. Volume 84, Issue 5.
- [15] Otabe, Y. and Kishi, T., 2005. Development of Hydration and Strength Model for Quality Evaluation of Concrete, *Industrial Science*, University of Tokyo, 57(2); pp.37-42.
- [16] Maekawa, K., Zhu, X., Chijiwa, N. and Tanabe, S., 2016. Mechanism of Long-Term Excessive Deformation and Delayed Shear Failure of Underground RC Box Culverts, *Journal of Advanced Concrete Technology*, Volume 14, Issue 5, May 2016; pp.183-204.
- [17] Ikeda, S., Uji, K., 1980. Studies on The Effect of Bond on The Shear Behavior of Reinforced Concrete Beams, *Journal of JSCE*, 293, January 1980; pp.101-109.